ChemComm

COMMUNICATION

View Article Online
View Journal | View Issue

Cite this: *Chem. Commun.*, 2022, 58, 13015

Received 24th September 2022,
Accepted 21st October 2022

DOI: 10.1039/d2cc05250d

rsc.li/chemcomm

The unique role of pore wall nanostructurization in the intrachannel photo-ATRP for fine-tuning PMMA tacticity†

Paulina Maksym, *[ab] Roksana Bernat, [bc] Kajetan Koperwas, [bd] Marcin Wojtyniak,[e] Julita Piecha,[bd] Barbara Hachuła, [bc] Monika Geppert-Rybczyńska,[bc] Agnieszka Brzózka,[f] Grzegorz D. Sulka, [f] Magdalena Tarnacka, [bd] Marian Paluch[bd] and Kamil Kamiński[bd]

In this paper, efficient MMA photo *O*-ATRP protocols conducted inside nanoreactors varying in nanostructured interfaces are reported for the first time. We showed that the microstructure of recovered polymers could be easily tuned just by implementing a given type of nanochannel (d = 10, 19–28, 35, 160 nm).

Soft matter confined at the nano/mesoscale level reveals a fascinating behaviour significantly deviating from that observed at the macroscale. It is due to the molecular ordering/packing variation that is strictly related to the additional interfacial interactions between host and guest molecules. Consequently, dynamic properties such as viscosity, diffusivity, glass transition temperature, thermal stability, conductivity, and morphology of the spatially restricted samples are strongly affected.[1,2]

Recently, there has been a growing interest in studying polymerization processes in spatially limited systems. In this context, it is noteworthy that the following intrachannel polymerization protocols: photo-,[3] and thermally-,[3] induced free-radical polymerization (FRP), photo-,[4] and thermally-,[5,6] induced reversible-addition fragmentation chain transfer polymerization (RAFT), ring-opening polymerization (ROP),[7] and polycondensation[8] have been reported in the literature so far. Remarkably, these elegant strategies utilized nano/mesoreactors in the form of silica- (SiO_2),[9–11] and aluminum oxide (AAO)[12–14] templates/plates, and metal–organic frameworks,[6,9,15] and zeolite[16] powders. Many experimental studies and simulations revealed that due to the specific interactions occurring at the interface, there is a higher local concentration of molecules, and reduced diffusivity of chains (in close proximity to the pore walls). What is more, a confined polymerization performed inside porous materials of ordinary morphology could (i) prevent side reactions/chain termination, (ii) cause a higher rate compared to the macroscale,[17] and (iii) be an effective tool for tuning macromolecules' molecular weight (M_n), dispersity ($Đ$), and stereoregularity, enabling at the same time to obtain topologically and mechanically unique polymers.[18,19] Moreover, having in mind that the interface has an enormous impact on the pathway of many physico-chemical processes, apart from the routine functionalization/silanization (making it more hydrophobic), it seems obvious to study the intrachannel polymerization utilizing more sophisticated mesoporous membranes (*i.e.*, of modified pore walls). This aspect is extremely important considering recent studies by some of us on the poly(propylene glycol) derivatives incorporated into AAO membranes of modulated pore diameter ($19 < d < 28$ nm), where we unexpectedly observed the bulk-like behaviour of material confined at the nanoscale.[20] This simple example shows that investigating the effect of nanostructurization, the roughness of pore walls on the polymerization path, and the macro-, and microstructure of resulting polymers is significant.

Herein, we demonstrate a facile macro- and nanoscale (intrachannel) organocatalyzed photo-ATRP protocol (*O*-ATRP) (Scheme 1).

For that purpose, the macroscale experiments were conducted in classical flasks, whereas for intrachannel *O*-ATRP, we selected the following types of mesoporous templates (a) type 1 – commercial, regularly ordered spherical pores (d = 10, 35, and 160 nm); (b) type 2 – self-produced, regularly ordered conical pores (d = 35 nm); and (c) type 3 – self-produced, regularly ordered pores of modulated pore diameter ($19 < d < 28$ nm). To our knowledge, this is the first report on polymerization utilizing mesoporous membranes of

[a] *Institute of Materials Engineering, University of Silesia, 75 Pulku Piechoty 1a Street, Chorzow 41-500, Poland. E-mail: paulina.maksym@us.edu.pl*
[b] *Silesian Center of Education and Interdisciplinary Research, University of Silesia, 75 Pulku Piechoty 1A Street, Chorzow 41-500, Poland*
[c] *Institute of Chemistry, University of Silesia, Szkolna 9 Street, Katowice 40-007, Poland*
[d] *Institute of Physics, University of Silesia, 75 Pulku Piechoty 1 Street, Chorzow 41-500, Poland*
[e] *Institute of Physics – Center for Science and Education, Silesian University of Technology, Krasińskiego 8 Street, Katowice 40-019, Poland*
[f] *Department of Physical Chemistry and Electrochemistry, Faculty of Chemistry, Jagiellonian University, Gronostajowa 2 Street, Krakow 30-387, Poland*
† Electronic supplementary information (ESI) available. See DOI: https://doi.org/10.1039/d2cc05250d

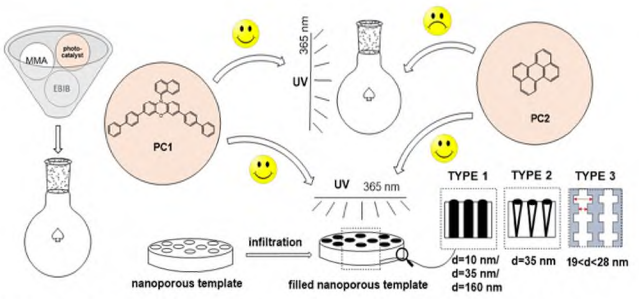

Scheme 1 Schematic outline of a facile MMA *O*-ATRP protocol.

different nanostructured interfaces. It is worth stressing that to date only a few strategies concerning normal ATRP, activator generated by electron transfer (AGET ATRP), and activator regenerated by electron transfer (ARGET ATRP) have been previously implemented in intrachanell[21] polymerization. Note that the vast majority of reports in the literature concern surface-initiated confined processes (SI-ATRP).[22,23] Within this work, methyl methacrylate (MMA) and ethyl α-bromoisobutyrate (EBiB) have been selected as the monomer and the initiator, respectively; whereas 3,7-di(4-biphenyl)-1-naphthalene-10-phenoxazine (PC1) and perylene (PC2) were selected as photoorganocatalysts (PCs). Reactions were conducted using a $[MMA]_0/[EBiB]_0/[PC]_0$ = 100/1/0.1 ratio, in anisole or DMF, at 298 K within 3 h. In the ESI,† we presented the setup for confined processes (Fig. S1, ESI†), synthetic procedures, emission-absorption spectra (Fig. S2, ESI†), and characteristics of membranes (Table S1, ESI†), and produced polymers (Fig. S3–S8, ESI†). Of particular note is that these PCs were previously used to promote MMA *O*-ATRP at the macroscale (white and blue LEDs) and reveal utterly different process control (PC1[24] – high control, PC2[25] – less control). In addition, they both required relatively long irradiation time to reach completed MMA consumption (8–24 h). Our main goal was to check whether several confined protocols proposed by us would (i) show a robust catalytic effect, (ii) increase the control over MMA PC2-mediated *O*-ATRP, and more exciting (iii) affect the properties of obtained polymers, including M_n, $Đ$, and tacticity.

As a starting reference point of our investigation, we performed PC1-mediated MMA *O*-ATRP at a macroscale which, after 3 h of UV irradiation at 298 K, produced well-defined PMMA with excellent agreement between theoretical and experimental M_n = 4.0 kg mol^{-1}, narrow $Đ$ = 1.10, and high initiation efficiency I^* = 92.6% (Table 1, entry 1). However, this experiment proceeded with moderate MMA consumption α = 39%. Next, we sought to assess the scope of PC1-operated *O*-ATRP nanopolymerizations. To our delight, the implementation of type 1 templates showed a dramatic beneficial effect on the reaction rate, giving complete MMA consumption after 3 h regardless of the pore size of the applied matrices. More encouragingly, as presented in Table 1, entries 2–4, the obtained nanomaterials were characterized by different parameters. In particular, as the template's pore size decreased,

Table 1 PC1-, and PC2-mediated ATRP at the macro-, and mesoscale

No	Reactor	d [nm]	α^a [%]	$M_{nth}{}^a$ [kg mol^{-1}]	$M_{nSEC}{}^b$ [kg mol^{-1}]	$Đ^b$
PC1-mediated *O*-ATRP						
1	Batch	—	39	3.9	4.0	1.10
2	Type 1	160	>99	9.9	6.7	1.17
3		35	>99	9.9	15.2	1.18
4		10	>99	9.9	17.8	1.12
5	Type 2	35	>99	9.9	12.3	1.18
6	Type 3	19–28	>99	9.9	10.7	1.32
PC2-mediated *O*-ATRP						
7	Batch	—	39	3.9	79.4	1.57
8	Type 1	160	>99	9.9	20.8	1.22
9		35	>99	9.9	21.8	1.34
10		10	>99	9.9	37.5	1.37
11	Type 2	35	>99	9.9	17.2	1.33
12	Type 3	19–28	>99	9.9	16.3	1.39

[a] Determined from ^{1}H NMR. [b] Determined from SEC-LALLS (DMF).

PMMA of higher M_n was formed, starting from 6.7 kg mol^{-1} (d = 160 nm), through 15.2 kg mol^{-1} (d = 35 nm), ending with 17.8 kg mol^{-1} (d = 10 nm) (I^* = 56–147%). Noteworthy, produced in this way, polymers were also characterized by low $Đ$ = 1.12–1.18, with the lowest recorded value for PMMA recovered from the type 1 template (d = 10 nm). Next, we explored *O*-ATRP using self-produced AAO-based matrices of different nanostructure interfaces. Pleasingly, the utilization of type 2 template (conical pore shapes) and type 3 template (modulated diameters) for the PC1-mediated process also caused complete MMA consumption within 3 h, delivering PMMAs of M_n = 12.3 kg mol^{-1} $Đ$ = 1.18 (I^* = 80%), and M_n = 10.7 kg mol^{-1} $Đ$ = 1.32 (I^* = 92%), respectively (Table 1, entries 5 and 6).

Having successfully produced PMMAs *via* the PC1-mediated *O*-ATRP system, our attention was next turned to the PC2-mediated one. In this instance, the UV-irradiated batch process proceeded to α = 39% with dramatically poor control and a very low initiation efficiency (I^* = 4.9%), yielding PMMA of significant deviation between theoretical and absolute M_n = 79.4 kg mol^{-1} ($Đ$ = 1.57) (Table 1, entry 7). On the other hand, reactions carried out inside mesoporous membranes proceeded with a higher control, which was reflected in lowering dispersities of PMMAs (Table 1, entries 8–12). Representative SEC-LALLS traces of polymers produced within PC1- and PC2-systems are presented in the ESI† (Fig. S3). Here, we also calculated the percentage of bromine chains employing ^{1}H NMR (Fig. S5, ESI†). The PC1-mediated process obtained PMMAs revealed 85–91% bromine-end groups, while for PC2, only 10%. The obtained results are in line with the FT-IR analysis. For the polymer produced within the PC2-mediated *O*-ATRP system, the peaks originating from the initiator are barely visible (Fig. S8a and b, ESI†). The above considerations are consistent with the results of chain-extension experiments with glycidyl methacrylate on PMMAs obtained at the macroscale (see Fig. S4 and S7, ESI†).

Interestingly, we observed an increase in PMMAs M_n for both PC-mediated experiments with a decrease in pore diameters. In fact, this result is directly related to the finite size

effect. Previous reports explain the phenomenon of obtaining higher M_n in nanopolymerization with reduced diffusivity of propagating chains. Floudas[26] and some of us[27] reported that segmental relaxation times (directly correlated to viscosity and diffusion) get shorter with decreasing pore diameter. Matyjaszewski, Antonietti, Schmidt *et al.*, in turn, combine the increasing MW with the compartmentalization effect.[21] The polymerization kinetics in confined conditions is accelerated due to the suppressed deactivation. They also claimed that the confined process predominately depends on the initiation stage having little relation to time (providing higher MW polymers). Other studies reported decreasing initiation efficiency in the very small nanopores delivering polymers of lower M_n compared to the macroscale.[17,18] Note that the lower initiation efficiency could also result from the differences in light penetration between the glassy vial and AAO-based templates. Our previous paper concerning intrachannel photo-RAFT utilizing different mesoporous templates demonstrates that a 50 μm thick AAO membrane absorbs 32% of incoming light. In contrast, the glass batch reactor with a thickness of 1500 μm absorbs 8% of incoming light at λ = 365 nm.[4]

Next, we examine whether spatially constrained media applied herein could tune PMMA tacticity. From sets of data presented in Table S2 and Fig. S6 (ESI†), we can conclude that (i) bulk PMMA is dominated by the syndiotactic-rich form (mm : mr : rr = 7.7% : 37.8% : 54.5%), (ii) samples recovered from type 1 templates show a dramatic increase of isotactic triads, with their highest content, noted for PMMA produced inside pores of d = 35 nm (mm : mr : rr = 63.3% : 11.4% : 25.3%), (iii) samples synthesized in type 2 membranes reveal increasing isotacticity (mm : mr : rr = 41.5% : 26.8% : 31.7%), although this change is not as significant as in the case of those produced under type 1 templates and (iv) PMMA recovered from type 3 templates is dominated by atactic triads with an equally significant contribution of syndiotactic (mm : mr : rr = 23.8% : 40.6% : 35.6%).

Moreover, to look deeper into the nature of observed tacticity changes, additional PC1-mediated experiments were performed at 308 K, 318 K, and 333 K allowing us to employ the absolute reaction rate theory and examine if syndiospecific propagation is governed by entropic or enthalpic factors (see the ESI†).[28] From Fig. 1, it can be observed that confinement evidently changes the temperature dependence of $\ln(P_m/P_r) = (\Delta S^i_{act} - \Delta S^s_{act})/R - (\Delta H^i_{act} - \Delta H^s_{act})/RT$.

For the bulk system, we obtain the positive values of both enthalpic and entropic factors. Polymerization carried out within type 1 drastically increases the entropic term's value, which implies an independent temperature factor preventing random propagation within the pore.[29] For polymerization in pores of type 2 and 3, we observe a significant increase in the entropic and enthalpic terms with respect to the bulk system. Both terms are comparable for the type 2 pore, whereas the entropic one evidently dominates within the type 3 pore. Generally, confined geometry more favours the formation of a less sterically bulky isotactic structure than that of a more sterically hindered atactic one. However, in some cases, (*e.g.*, in MOFs of very small pore diameters), limited improvements in isotacticity can be observed.[21] In our case, PMMAs produced

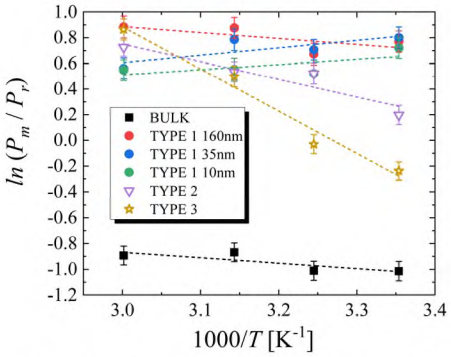

Fig. 1 The dependence of isotactic to syndiotactic diad ratio on temperature for PMMA synthesized at macro- and nanoscale.

inside templates of d = 10 nm showed the lowest content of isotactic fractions among all recovered from type 1, although still higher than those reported up to now in the literature. Note that the stereoregularity of forming nanomaterials is also strongly influenced by interactions between monomer, solvent, orienting propagating chains and the surface chemistry.[19]

Nevertheless, to better understand these observations, we took a closer look at the chemical nature of the MMA and applied solvents (anisole, DMF), especially their wettability to the AAO. Interestingly, our recent measurements of MMA in terms of the contact angle, θ revealed that it is 0 [°] at 298 K.[3] Consequently, it wets the AAO surface very well and strongly adheres to the pore walls. Similar results were found for both investigated herein solvents; the θ of anisole and DMF reaching value 0 [°] (see the ESI,† Fig. S9), and 9.9 [°],[30] respectively. Hence, in such systems, the adhesive force is strong enough to overcome the cohesive force making it easier to fulfil pores (good solvents to this template). Thus, we can suppose that the PCs-mediated system investigated herein revealed a similar surface chemistry. Moreover, to assess the influence of the templates' surface roughness on the parameters of the obtained polymers, at least to a small extent, we performed unique measurements using AFM. We measured membranes of similar pore diameters but varying in nanostructure interfaces: type 1 (d = 35 nm) and 3 (19 < d < 28 nm). Unfortunately, due to the specificity of the preparation of the type 2 template, it was not possible to perform AFM analyses for them. Using an ultra-sharp tip, we were able to measure the inner roughness parameter of the empty pores in templates in the nanoscale (all procedures are presented in the ESI†). The schematic of a pore structure, along with the AFM approach is shown in Fig. 2. We have calculated RMS values along vertical lines using only the data from the pore internal wall (the masked regions). Thus, we were able to obtain a linear RMS (l-RMS), that is not influenced by the horizontal high changes (pores curvature) and can be used for comparison between membranes.

The measurement showed that the surface roughness (l-RMS parameter) of the membrane type 1 is around ~2.97 nm that is very close to that estimated for type 3 (around ~2.5 nm). Typically, higher surface roughness leads to stronger polymer adsorption as the random walk of the polymer chain

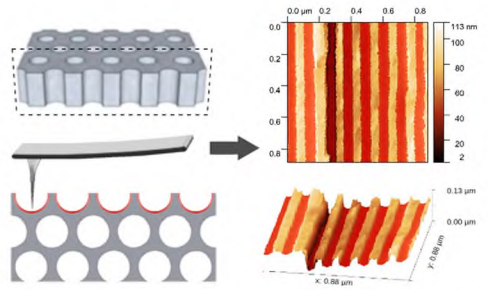

Fig. 2 Typical data of topography of type 1 and type 3 templates, along with the 3d image of the surface.

has a higher probability to come into contact with the surface. Thus, it is possible to connect changes in tacticity to surface roughness. We assume that overall tacticity calculated for PMMA recovered from the type 3 template was superimposed by the two confined effects: finite size and pore walls nanostructurization. Nonetheless, to better understand the impact of both aspects on the tacticity of the resulting polymers, more simulations and experimental data should be carried out.

As illustrated, one of the great benefits of the *O*-ATRP confined methodology proposed herein is that complete MMA consumption can be reached in a relatively short time (3 h) regardless of mesoporous membrane types. We were also delighted to find that PMMA tacticity can be tuned upon nanopolymerization just by simply using a given type of nanoreactor. We also found that PMMAs of higher MW could be produced when pore diameters of the type 1 mesoporous template decreased. In the case of stereoregularity control, our protocols are alternatives to FRP in the presence of fluoroalcohols/Lewis acid additives or when supported by a high electric field.[31]

P. M. and R. B. are thankful for financial support from the Polish National Science Centre within the SONATA project (DEC-2018/31/D/ST5/03464).

Conflicts of interest

There are no conflicts to declare.

References

1 S. Perkin and J. Klein, *Soft Matter*, 2013, **9**, 10438–10441.
2 D. Richter and M. Kruteva, *Soft Matter*, 2019, **15**, 7316–7349.
3 M. Tarnacka, P. Maksym, A. Zięba, A. Mielańczyk, M. Geppert-Rybczyńska, L. Leon-Boigues, C. Mijangos, K. Kamiński and M. Paluch, *Chem. Commun.*, 2019, **55**, 6441–6444.
4 R. Bernat, P. Maksym, M. Tarnacka, A. Szelwicka, R. Bielas, M. Wojtyniak, K. Balin, B. Hachuła, A. Chrobok, M. Paluch and K. Kamiński, *Polym. Chem.*, 2021, **12**, 1105–1113.
5 P. Maksym, M. Tarnacka, K. Wolnica, A. Dzienia, K. Erfurt, A. Chrobok, A. Zięba, R. Bielas, K. Kaminski and M. Paluch, *Polym. Chem.*, 2018, **9**, 335–345.
6 J. Hwang, H. C. Lee, M. Antonietti and B. V. K. J. Schmidt, *Polym. Chem.*, 2017, **8**, 6204–6208.
7 M. Tarnacka, A. Dzienia, P. Maksym, A. Talik, A. Zięba, R. Bielas, K. Kaminski and M. Paluch, *Macromolecules*, 2018, **51**, 4588–4597.
8 B. Sanz, N. Ballard, Á. Marcos-Fernández, J. M. Asua and C. Mijangos, *Polymer*, 2018, **140**, 131–139.
9 M. Choi, F. Kleitz, D. Liu, Y. L. Hee, W. S. Ahn and R. Ryoo, *J. Am. Chem. Soc.*, 2005, **127**, 1924–1932.
10 Q. Tian, H. Zhao and S. L. Simon, *Polymer*, 2020, **205**, 122868.
11 T. Kinsey, K. Glynn, T. Cosby, C. Iacob and J. Sangoro, *ACS Appl. Mater. Interfaces*, 2020, **12**, 44325–44334.
12 M. Tarnacka, A. Chrobok, K. Matuszek, S. Golba, P. Maksym, K. Kaminski and M. Paluch, *ACS Appl. Mater. Interfaces*, 2016, **8**, 29779–29790.
13 L. León-Boigues, C. von Bilderling, L. Pietrasanta, O. Azzaroni, C. Mijangos and J. M. Giussi, *ACS Appl. Polym. Mater*, 2021, **3**(2), 640–650.
14 B. Sanz, N. Ballard, J. M. Asua and C. Mijangos, *Macromolecules*, 2017, **50**, 811–821.
15 X. Xu, Y. Zeng, C. Yu and F. Zhang, *J. Porous Mater.*, 2020, **27**, 95–105.
16 S. M. Ng, S. I. Ogino, T. Aida, K. A. Koyano and T. Tatsumi, *Macromol. Rapid Commun.*, 1997, **18**, 991–996.
17 M. Michailidis, G. D. Verros, E. A. Deliyanni, E. G. Andriotis and D. S. Achilias, *J. Polym. Sci., Part A: Polym. Chem.*, 2017, **55**, 1433–1441.
18 T. Uemura, Y. Ono, K. Kitagawa and S. Kitagawa, *Macromolecules*, 2008, **41**, 87–94.
19 H. Zhao and S. L. Simon, *Polymer*, 2020, **211**, 123112.
20 M. Tarnacka, M. Wojtyniak, A. Brzózka, A. Talik, B. Hachuła, E. Kamińska, G. D. Sulka, K. Kaminski and M. Paluch, *Nano Lett.*, 2020, **20**, 5714–5719.
21 H. C. Lee, J. Hwang, U. Schilde, M. Antonietti, K. Matyjaszewski and B. V. K. J. Schmidt, *Chem. Mater.*, 2018, **30**, 2983–2994.
22 C. B. Gorman, R. J. Petrie and J. Genzer, *Macromolecules*, 2008, **41**, 4856–4865.
23 J. M. Giussi, I. Blaszczyk-Lezak, M. S. Cortizo and C. Mijangos, *Polymer*, 2013, **54**, 6886–6893.
24 B. G. McCarthy, R. M. Pearson, C. H. Lim, S. M. Sartor, N. H. Damrauer and G. M. Miyake, *J. Am. Chem. Soc.*, 2018, **140**, 5088–5101.
25 G. M. Miyake and J. C. Theriot, *Macromolecules*, 2014, **47**, 8255–8261.
26 S. Alexandris, P. Papadopoulos, G. Sakellariou, M. Steinhart, H. J. Butt and G. Floudas, *Macromolecules*, 2016, **49**, 7400–7414.
27 M. Tarnacka, A. Talik, E. Kamińska, M. Geppert-Rybczyńska, K. Kaminski and M. Paluch, *Macromolecules*, 2019, **52**, 3516–3529.
28 J. W. L. Fordham, *J. Polym. Sci.*, 1959, **39**(135), 321–334.
29 F. A. Bovey and G. V. D. Tiers, *J. Polym. Sci.*, 1960, **44**(143), 173–182.
30 R. Redón, A. Vázquez-Olmos, M. E. Mata-Zamora, A. Ordóñez-Medrano, F. Rivera-Torres and J. M. Saniger, *J. Colloid Interface Sci.*, 2005, **287**, 664–670.
31 K. Chat, P. Maksym, K. Kamiński and K. Adrjanowicz, *Chem. Commun.*, 2022, **58**, 5653–5656.

